Supporting Information for

Structures, Magnetochemistry, Spectroscopy, Theoretical Study and Catechol Oxidase Activity of Dinuclear and Dimer-of-Dinuclear Mixed-Valence $Mn^{III}Mn^{II}$ Complexes Derived from a Macrocyclic Ligand

Arpita Jana, Núria Aliaga-Alcalde, Eliseo Ruiz,* and Sasankasekhar Mohanta*

Table S1. Selected structural parameters (distances in Å and angles in deg.) of $[\{Mn^{III}Mn^{II}L(\mu\text{-}O_2CEt)(EtOH)\}_2(\mu\text{-}O_2CEt)](ClO_4)_3$ (**3**)

Unit-I		**Unit-II**	
Mn1–O1	1.919(2)	Mn4–O8	1.903(2)
Mn1–O2	1.8890(19)	Mn4–O9	1.925(2)
Mn1–O3	2.101(2)	Mn4–O11	2.100(2)
Mn1–O5	2.341(3)	Mn4–O12	2.313(3)
Mn1–N1	1.990(2)	Mn4–N7	2.004(3)
Mn1–N2	2.000(3)	Mn4–N8	1.997(2)
Mn2–O1	2.271(2)	Mn3–O7	2.161(2)
Mn2–O2	2.374(2)	Mn3–O8	2.340(2)
Mn2–O4	2.124(3)	Mn3–O9	2.297(2)
Mn2–O6	2.136(3)	Mn3–O10	2.105(3)
Mn2–N3	2.240(3)	Mn3–N5	2.188(3)
Mn2–N4	2.206(2)	Mn3–N6	2.231(3)
Mn1···Mn2	3.2081(6)	Mn3···Mn4	3.2256(6)
O1–Mn1–N2	173.58(10)	O8–Mn4–N8	175.40(11)
O2–Mn1–N1	174.88(11)	O9–Mn4–N7	174.25(10)
O3–Mn1–O5	179.27(11)	O11–Mn4–O12	176.30(10)
O1–Mn1–N1	89.98(10)	O8–Mn4–N7	91.58(10)
O1–Mn1–O2	85.04(9)	O8–Mn4–O9	85.15(9)
O1–Mn1–O3	94.73(10)	O8–Mn4–O11	95.07(10)
O1–Mn1–O5	85.98(10)	O8–Mn4–O12	87.42(9)
O2–Mn1–N2	91.77(10)	O9–Mn4–N8	90.42(10)
O2–Mn1–O3	94.06(9)	O9–Mn4–O11	95.85(10)
O2–Mn1–O5	86.14(9)	O9–Mn4–O12	87.07(10)
O3–Mn1–N1	87.52(11)	O11–Mn4–N7	89.14(11)
O3–Mn1–N2	91.04(11)	O11–Mn4–N8	86.62(10)
O5–Mn1–N1	92.33(11)	O12–Mn4–N7	88.06(11)
O5–Mn1–N2	88.25(11)	O12–Mn4–N8	91.10(10)
N1–Mn1–N2	93.07(11)	N7–Mn4–N8	92.73(11)
O1–Mn2–N3	79.13(9)	O7–Mn3–N5	91.18(9)
O1–Mn2–N4	127.09(9)	O7–Mn3–N6	86.71(10)
O1–Mn2–O2	67.25(7)	O7–Mn3–O8	147.49(9)
O1–Mn2–O4	96.53(9)	O7–Mn3–O9	137.59(8)
O1–Mn2–O6	101.99(8)	O7–Mn3–O10	80.38(10)
O2–Mn2–N3	118.07(10)	O8–Mn3–N5	78.96(8)
O2–Mn2–N4	77.53(8)	O8–Mn3–N6	122.93(9)
O2–Mn2–O4	77.70(9)	O8–Mn3–O9	67.88(7)
O2–Mn2–O6	154.75(10)	O8–Mn3–O10	81.16(9)
O4–Mn2–N3	159.20(12)	O9–Mn3–N5	126.99(9)
O4–Mn2–N4	113.46(11)	O9–Mn3–N6	79.08(9)
O4–Mn2–O6	81.15(12)	O9–Mn3–O10	88.18(9)
O6–Mn2–N3	79.92(12)	O10–Mn3–N5	126.95(11)
O6–Mn2–N4	124.15(10)	O10–Mn3–N6	144.11(12)
N3–Mn2–N4	84.52(10)	N5–Mn3–N6	86.36(11)
Mn1–O1–Mn2	99.61(9)	Mn3–O8–Mn4	98.44(8)
Mn1–O2–Mn2	96.98(8)	Mn3–O9–Mn4	99.26(9)

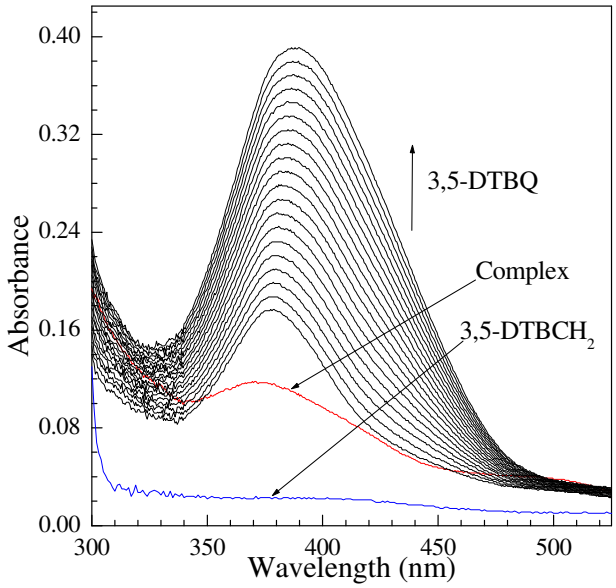

Figure S1. The spectral profile showing the increase of quinone band at 390 nm after the addition of 100 fold of 3,5-DTBCH$_2$ to a solution containing complex **1** (1×10^{-5} M) in MeOH. The first spectrum of complex + 3,5-DTBCH$_2$ mixture was recorded within one minute after mixing. The next spectra were recorded after each 3 minutes.

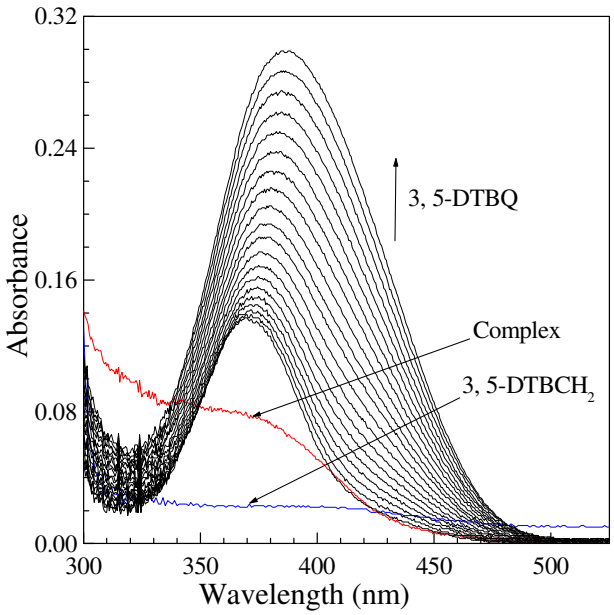

Figure S2. The spectral profile showing the increase of quinone band at 389 nm after the addition of 100 fold of 3,5-DTBCH$_2$ to a solution containing complex **2** (1×10^{-5} M) in MeCN. The first spectrum of complex + 3,5-DTBCH$_2$ mixture was recorded within one minute after mixing. The next spectra were recorded after each 3 minutes.

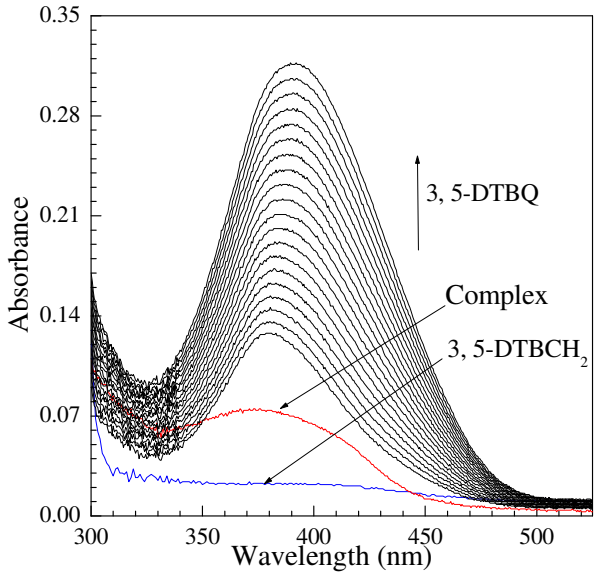

Figure S3. The spectral profile showing the increase of quinone band at 390 nm after the addition of 100 fold of 3,5-DTBCH$_2$ to a solution containing complex **2** (1×10^{-5} M) in MeOH. The first spectrum of complex + 3,5-DTBCH$_2$ mixture was recorded within one minute after mixing. The next spectra were recorded after each 3 minutes.

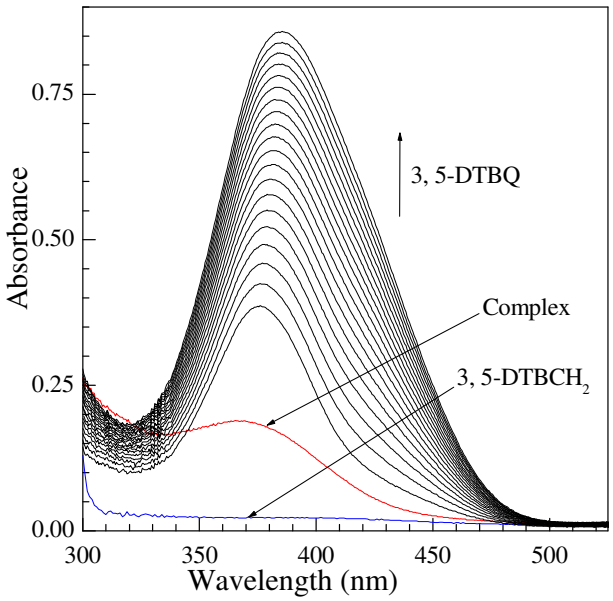

Figure S4. The spectral profile showing the increase of quinone band at 385 nm after the addition of 100 fold of 3,5-DTBCH$_2$ to a solution containing complex **3** (1×10^{-5} M) in MeCN. The first spectrum of complex + 3,5-DTBCH$_2$ mixture was recorded within one minute after mixing. The next spectra were recorded after each 3 minutes.

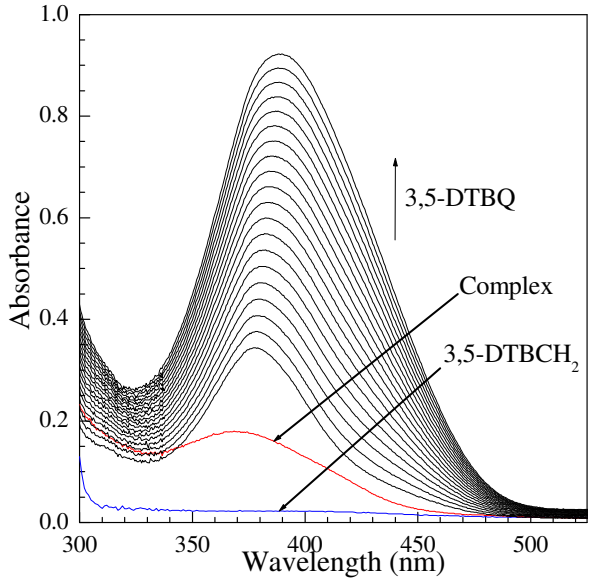

Figure S5. The spectral profile showing the increase of quinone band at 390 nm after the addition of 100 fold of 3,5-DTBCH$_2$ to a solution containing complex **3** (1×10^{-5} M) in MeOH. The first spectrum of complex + 3,5-DTBCH$_2$ mixture was recorded within one minute after mixing. The next spectra were recorded after each 3 minutes.

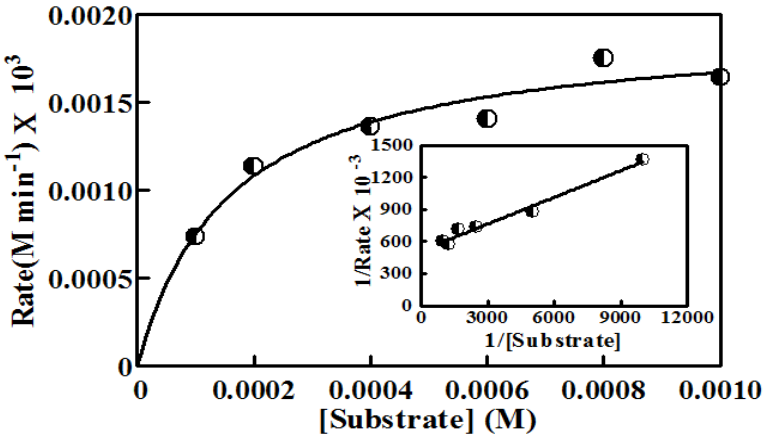

Figure S6. Initial rates versus substrate concentration for the 3,5-DTBCH$_2$→3,5-DTBQ oxidation reaction catalyzed by complex **1** in MeOH. Inset shows Lineweaver-Burk plot. Symbols and solid lines represent the observed and simulated profiles, respectively.

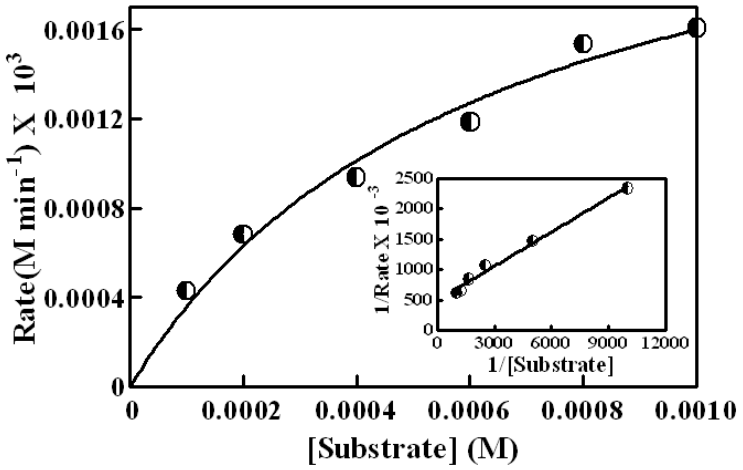

Figure S7. Initial rates versus substrate concentration for the 3,5-DTBCH$_2$→3,5-DTBQ oxidation reaction catalyzed by complex **2** in MeCN. Inset shows Lineweaver-Burk plot. Symbols and solid lines represent the observed and simulated profiles, respectively.

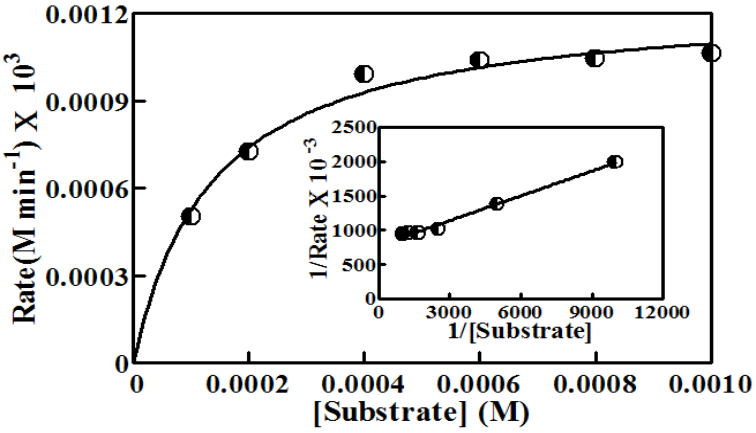

Figure S8. Initial rates versus substrate concentration for the 3,5-DTBCH$_2$→3,5-DTBQ oxidation reaction catalyzed by complex **2** in MeOH. Inset shows Lineweaver-Burk plot. Symbols and solid lines represent the observed and simulated profiles, respectively.

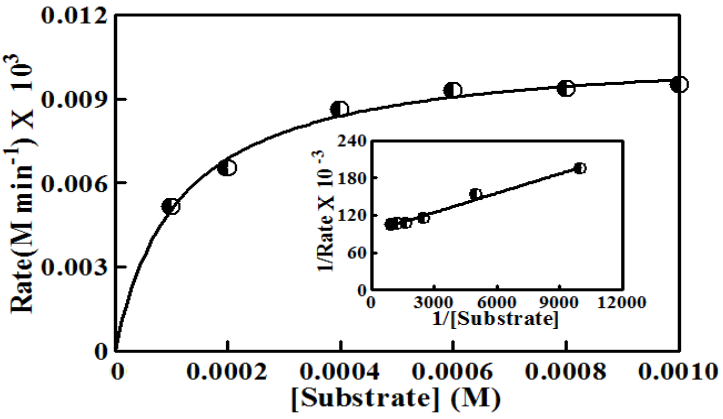

Figure S9. Initial rates versus substrate concentration for the 3,5-DTBCH$_2$→3,5-DTBQ oxidation reaction catalyzed by complex **3** in MeCN. Inset shows Lineweaver-Burk plot. Symbols and solid lines represent the observed and simulated profiles, respectively.

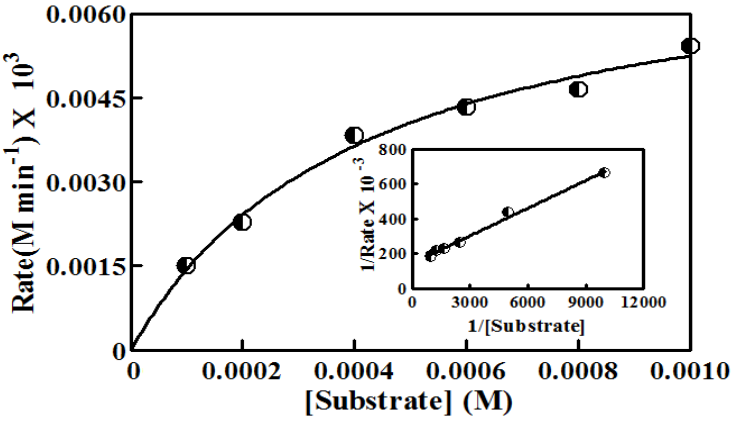

Figure S10. Initial rates versus substrate concentration for the 3,5-DTBCH$_2$→3,5-DTBQ oxidation reaction catalyzed by complex **3** in MeOH. Inset shows Lineweaver-Burk plot. Symbols and solid lines represent the observed and simulated profiles, respectively.

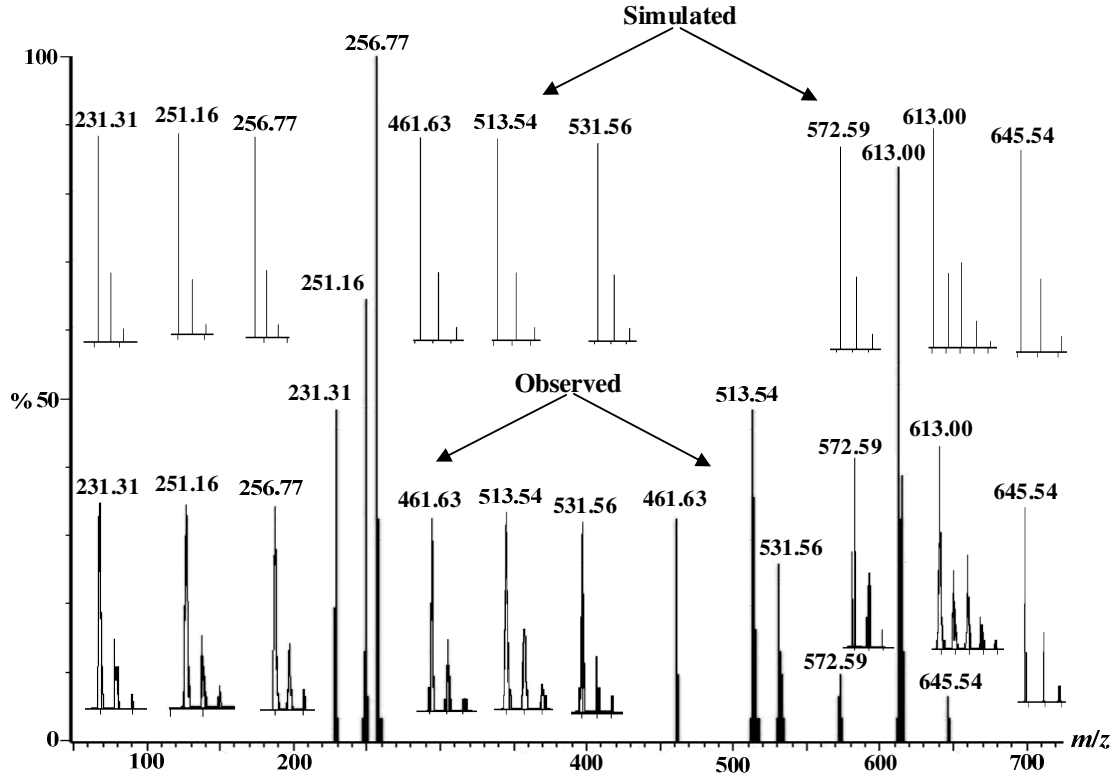

Figure S11. Electrospray ionization mass spectrum (ESI-MS positive) of $[Mn^{III}Mn^{II}L(\mu\text{-}O_2CMe)(H_2O)_2](ClO_4)_2{\cdot}H_2O{\cdot}MeCN$ (**1**) in MeCN showing observed and simulated isotopic distribution pattern.

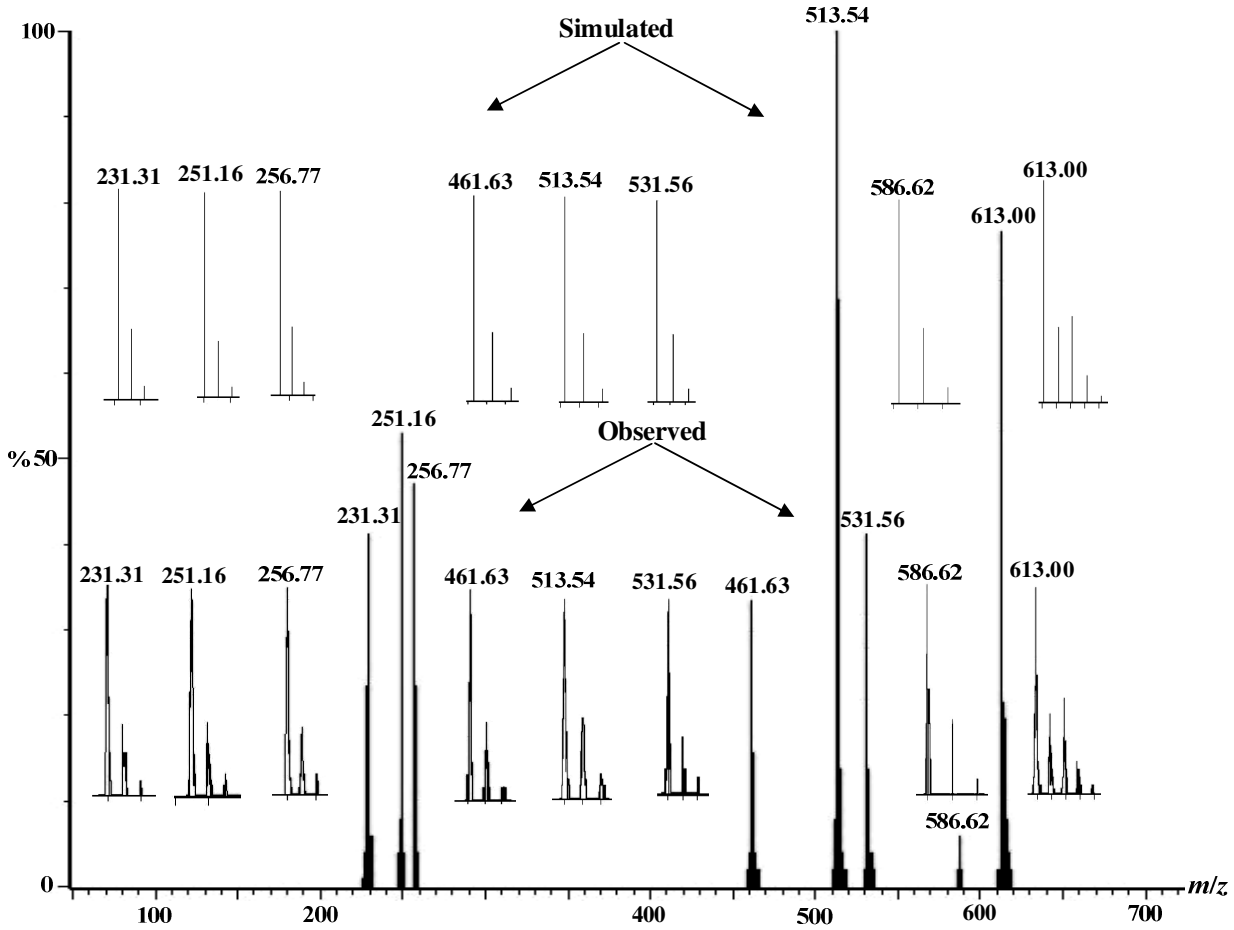

Figure S12. Electrospray ionization mass spectrum (ESI-MS positive) of [{$Mn^{III}Mn^{II}$L(μ-O_2CEt)(EtOH)}$_2$(μ-O_2CEt)](ClO_4)$_3$ (**3**) in MeCN showing observed and simulated isotopic distribution pattern.

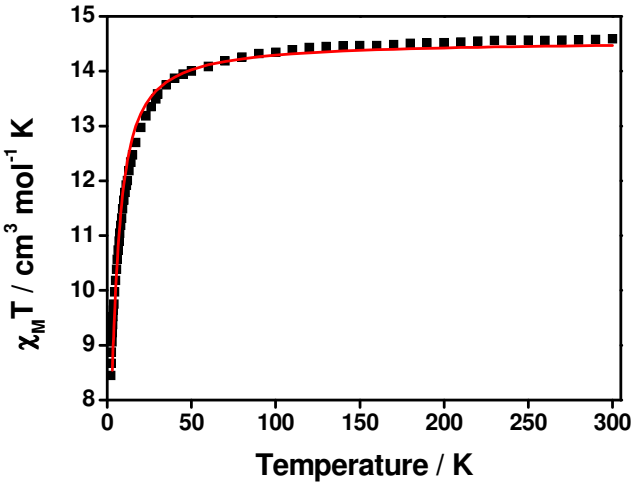

Figure S13. $\chi_M T$ vs T plot for compound $[\{Mn^{III}Mn^{II}L(\mu\text{-}O_2CEt)(EtOH)\}_2(\mu\text{-}O_2CEt)](ClO_4)_3$ (**3**) between 2.0 and 300.0 K. The experimental data are shown as black square dots and the red line corresponds to the theoretical values.

Information about ground state, first excited state, and first excitation energy of complexes 1–3

Due to the mixture of spin states because of the anisotropy of the systems we conclude the following magnetic information:

Complex 1:	
Degenerate ground state:	99.0% (2.0,2.5) or (−2.0,−2.5)
First excited state also degenerate:	57.5% (2.0,1.5) + 40.7% (−2.0,−1.5) or 57.5% (−2.0,−1.5) + 40.7% (2.0,1.5)
First excitation energy:	0.42 cm^{-1}
Complex 2:	
Degenerate ground state:	98.1% (2.0,−2.5) or (−2.0,2.5)
First excited state also degenerate:	96.6% (2.0,−1.5) or (−2.0,1.5)
First excitation energy:	0.63 cm^{-1}
Complex 3:	
Nondegenerate ground state:	40.4% (−2,−2.5,2.5,2) + 7% (−2,−1.5,1.5,2) + 40.4% (2,2.5,−2.5,−2) + 7% (2,1.5,−1.5,−2)
First excited state is degenerate:	25.1% (−2,−2.5,1.5,2) + 8.8% (−2,−2.5,2.5,1) + 8.9% (−2,−1.5,0.5,2) or 25.1% (2,2.5,−1.5,−2) + 8.8% (2,2.5,−2.5,−1) + 8.9% (2,1.5,−0.5,−2)
First excitation energy	0.03 cm^{-1}

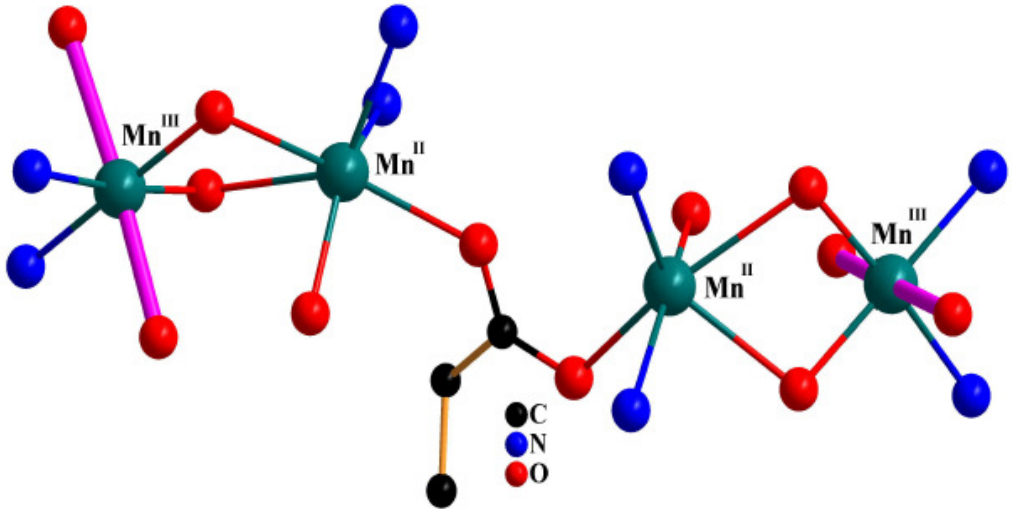

Figure S14. Scheme of the central core of compound **3** where most of ligands, counterions, and peripheral atoms have been removed for clarity. Jahn-Teller axes for both Mn^{III} centers are remarked in pink.